Nano- and Microporous Layer-by-Layer Assemblies Containing Linear Poly(ethylenimine) and Poly(acrylic acid)

Jodie L. Lutkenhaus,† Kathleen McEnnis, and Paula T. Hammond*

Department of Chemical Engineering, Massachusetts Institute of Technology, 77 Massachusetts Avenue 66-546, Cambridge, Massachusetts 02139

Received January 1, 2008; Revised Manuscript Received June 5, 2008

ABSTRACT: The structure and morphology as well as the mechanism of formation of porous polyelectrolyte multilayers consisting of linear poly(ethylenimine) (LPEI) and poly(acrylic acid) (PAA) have been systematically investigated as a function of pH. The structures obtained exhibit dramatic differences with small changes in the pH of multilayer assembly and pH of postassembly treatment, yielding an observed range of pore sizes from tens of nanometers to micrometers and pore volume fractions from 0 to 77%. The porous phase transition is quite rapid (<20 min), and structures observed include asymmetric membranes and isolated craters. It is thought that asymmetric membranes are achieved due to the high mobility of LPEI, which can exhibit interdiffusion when layered with PAA. To further understand the nature of the porous LbL multilayers, the pores were filled with liquid electrolyte and the impedance response of electrolyte-filled porous multilayers was examined; two time constants or two dry-state room temperature conductivities on the order of 10^{-6} and 10^{-9} S cm^{-1} were observed. The asymmetric membrane LbL structure, first reported here, holds many potential applications in terms of filtration, catalysis, drug delivery, etc.

Introduction

Porous materials and coatings possess excellent qualities (e.g., high surface area, tortuosity) for applications such as separations, drug delivery, catalysis, optics, and tissue scaffolding.[1–11] In a desire to design functional ultrathin porous films, key factors such as pore size, porosity, surface roughness, and film thickness must be precisely manipulated. A potential means of controlling these factors is based upon the layer-by-layer (LbL) assembly technique, where polyelectrolytes of opposite charge are alternately directed to a surface.[12,13] The advantages of this methodology are numerous: (1) conformal coatings of challenging geometries are possible,[14–16] (2) ultrathin films are achievable because the thickness of each film is controlled by the number of LbL cycles (angstroms to nanometers per cycle),[13] and (3) the properties of each film are finely controlled and tuned by assembly conditions such as pH and ionic strength.[17–19] Reported applications of porous LbL assemblies include Bragg reflectors,[20] drug delivery,[21] superhydrophobic films,[22,23] antireflection films,[24] molecular memory,[25] and sacrificial templating.[26,27] Nano- and microporous layer-by-layer assemblies are created using a simple procedure developed by Rubner and coworkers.[28] First, LbL assembly of weak polyelectrolytes (often poly(allylamine hydrochloride) (PAH) and poly(acrylic acid)) is performed under conditions where both polyelectrolytes are partially charged, resulting in smooth and continuous films. Following assembly, the LbL film is immersed in a bath of acidic solution, and the formation of a porous architecture is observed. The porous transition, marked by a significant increase in film thickness and roughness, is credited to the change in charge density along constituent polyelectrolyte backbones and subsequent ionic bond disruption and re-formation.[28] Another model for pore formation points to the loss of polyelectrolyte from the LbL film during the postassembly treatment step.[29] Alternative methods for creating porous LbL films, such as using mesoporous silica templates, are described by Caruso and coworkers.[30–36]

In recent work,[37,38] porous multilayers consisting of linear poly(ethylenimine) (LPEI) and poly(acrylic acid) (PAA) were described, where these films were used as a porous support for oligo(ethylene glycol) dicarboxylic acid (OEGDA) electrolyte in a dye-sensitized solar cell. These early reports used partially charged weak polyelectrolytes LPEI and PAA, both at pH 5.0, which are known to give thick and lightly electrostatically cross-linked multilayers (30 nm/cycle).[39] When the LPEI/PAA LbL films were immersed in water of pH less than 3.0, the film thickness nearly tripled and a porous morphology was observed. At ambient conditions, the reported conductivity of the OEGDA-filled porous LbL assembly was $10^{-6}-10^{-5}$ S cm^{-1},[37,38] which was 100 times higher than its nonporous counterpart.[39] Using such a porous LbL film as an electrode separator and electrolyte support has a distinct advantage in that it can be made quite thin (<1 μm), whereas conventional separators or supports for liquid electrolyte are 25 μm thick.[40] In general, porosity in ultrathin films is of interest for numerous applications, depending on the structure and morphology of the film. Ionic conductors require high interconnectivity between pores; on the other hand, porous systems developed for low dielectric media often require isolated, air-filled pockets that do not enable adsorption of water or other impurities. Microfiltration membranes require micron-scale homogeneous porous media, whereas ultrafiltration membranes are generally asymmetric systems with a nanoporous skin layer and a microporous bulk layer.

To design LbL systems as porous media with the desired level of control, it is important to understand the kinetics and mechanism of pore formation and the conditions that yield different pore sizes, pore size distributions, and pore morphologies. For example, in multilayer systems that exhibit nonlinear film growth during assembly due to polycation interdiffusion, there is an added potential of forming gradient porous thin films or asymmetric structures under appropriate conditions; such films may also offer interesting potential applications. As of yet, the effect of assembly pH and postassembly pH treatment conditions upon the structure and morphology of LPEI/PAA LbL films has remained largely unexplored.

Here, it was desired to investigate and control the formation and structure of porous LPEI/PAA multilayers systematically

* Corresponding author. E-mail: hammond@mit.edu.
† Current address: Department of Chemical Engineering, Yale University, New Haven, CT.

10.1021/ma800003x CCC: $40.75
Published on Web 07/23/2008

as a function of pH treatment and assembly conditions, to better understand their potential as separation membranes, dielectric media, reactive substrates, and/or electrolyte supports. Unique to the LPEI/PAA multilayer system is the fact that the pK_a of LPEI is less than that of PAH, meaning that LPEI is more responsive to changes in pH; also, multilayer films containing LPEI exhibit greater interdiffusion and exchange relative to PAH systems, which suggests a higher mobility of the polycation LPEI.[41–46] For this reason, it is expected that the porous transition in LPEI/PAA LbL systems will occur more quickly (because of a higher polycation mobility) than PAH/PAA LbL systems and will yield different morphologies and pore structures (because of pronounced interdiffusion of LPEI).

In this work we investigate the structure, formation, and ion transport capabilities of LPEI/PAA LbL multilayer films. The latter studies were used to yield an idea of the interconnectivity of the different structures generated in the porous LbL films as a function of pH. A range of assembly pH (3−6) and postassembly treatment pH (1.75−3.00) is examined to elucidate the impact on pore volume, pore size, and surface roughness. Pore volumes reaching ≈80% and pore sizes ranging from tens of nanometers to microns were achieved by modulating assembly and treatment pH. In some cases, the porous transition occurred in less than 2 min of postassembly treatment time. The data support that this porous transition is attributed to the neutralization of PAA and the ionization of LPEI within the LbL assembly, where changes in polyelectrolyte charge density ultimately control the extent of electrostatic cross-linkage and the charge buildup within the film. AFM and SEM imaging reveal a variety of structures including nanoporous films, asymmetric membranes, and isolated craterlike micron-scale pores as treatment pH increases from 1.75 to 3.00. To the best of the authors' knowledge, this is the first observation of asymmetric membrane structure in porous LbL assemblies; the resulting composite membrane structure, consisting of a fine, porous top layer and an underlying macroporous layer, is of great technological interest for separations and other relevant applications. Electrochemical impedance spectroscopy, a technique that is useful for measuring conductivity and determining ion transport characteristics, was performed on nonporous and porous LPEI/PAA multilayers soaked in a nonaqueous electrolyte. Porous multilayers exhibited two semicircles and two time constants, whereas nonporous multilayers yielded one. The two time constants were linked to the presence of two phases (liquid-filled pores and LbL matrix), and two dry state room temperature conductivities were calculated (10^{-6} and 10^{-9} S cm^{-1}). Structures observed here may be implemented as functional films for a variety of future applications.

Materials and Methods

Solution Preparation. 0.02 M linear poly(ethylenimine) (LPEI) of molecular weight (MW) 25 000 g/mol and 0.02 M poly(acrylic acid) (PAA) of MW 90 000 g/mol were made using polymer as received from Polysciences and Milli-Q 18 MΩ water. Prior to use, solutions were vacuum-filtered. Polymer solution pH was adjusted to pH 3, 4, 5, or 6 using hydrochloric acid. Solution pH was monitored using Beckman Coulter electrodes that were calibrated within minutes of use and cleaned within 1 week of use in order to minimize error (±0.01 pH units).

Layer-by-Layer Film Assembly. Films were constructed using a modified programmable Carl Zeiss HMS slide stainer. Silicon substrates were cleaned with piranha solution for 5 min (30:70 v/v H_2O_2:H_2SO_4) and rinsed with Milli-Q water. (*Caution: piranha solution is corrosive, and proper personal protective equipment must be worn.*) ITO-coated glass substrates were cleaned with 15 min intervals of sonication in dichloromethane, acetone, methanol, and Milli-Q water. Immediately before assembly, substrates (silicon, ITO-coated glass) were oxygen plasma treated for 2 min. The substrate was first dipped in pH-adjusted LPEI solution for 15 min and rinsed with agitation in Milli-Q water for 2 min, followed by two 1 min rinses. Then, the substrate was exposed to pH-adjusted PAA solution for 15 min and rinsed as before. Both polyelectrolyte solutions were held at the same pH. The procedure was repeated 30 times to give a film of 30 layer pairs. LbL films were dried using an air gun and stored in a desiccator filled with phosphorus pentoxide until further treatment. Films assembled at pH x will be referred to as "pH x LPEI/PAA films", where x was varied from pH 3 to 6. Film thickness was measured using a Tencor P-10 profilometer; a groove in the film was made using a razor blade, and the profilometer stylus measured the depth of the groove to give the film thickness. The thickness was recorded three times at different locations and averaged to yield one data point; the standard deviation of the combined measurements was taken as the error. For surface roughness measurements, the root-mean-square (rms) surface roughness was measured along a path greater than 300 μm. The rms roughness was recorded three times in different locations and averaged as before.

Postassembly Treatment of Layer-by-Layer Films. An as-made pH x LPEI/PAA film was exposed to pH-adjusted Milli-Q water of pH 1.75, 2.00, 2.50, 2.75, or 3.00 for 20 min, unless otherwise stated. pH adjustment was performed using hydrochloric acid as before. Immediately following postassembly treatment, the film was dipped in Milli-Q water for 15 s or less. The resulting film was thermally cross-linked via amidation[47] in a 120 °C convection oven for 1 h and stored in a desiccator until further characterization.

AFM. A Dimension 3100 AFM by DI Instruments with a Nanoscope 3A controller in tapping mode was used to investigate surface morphology of the LbL films on silicon. NCH Pointprobe AFM cantilevers were purchased from Pacific Nanotechnologies. All films were 30 layer pairs thick. The tip radius of curvature was 10 nm, as indicated by the manufacturer.

SEM. Images were captured using a JEOL-5910 SEM system operating at 2−5 keV. 100 Å of Au−Pd was sputter-deposited on the samples prior to imaging to suppress charging. Cross-section images were taken from samples immersed in liquid nitrogen and cleaved with a diamond scribe (i.e., freeze-fractured). Some cross-sectional images were imaged while tilted to improve clarity.

Impedance Spectroscopy. Impedance spectroscopy using a Solartron 1260 was performed on a solid-state LbL cell for cross-plane (z-direction) measurements. The construction of the cell is described elsewhere by DeLongchamp and Hammond.[39] Briefly, an LbL film was constructed on a substrate of ITO-coated glass, and then the postassembly treatment step was applied. Patterned gold electrodes, 100 nm thick and 2 mm wide, were then thermally evaporated using an Edwards Auto 306 at 0.08 nm/s. Copper tape from 3M was applied to the gold to form a contact pad. The active area was 6 mm^2, and the LbL film consisted of 30 layer pairs. Following gold evaporation, the edge of the LbL-coated ITO slide was immersed in a dish of electrolyte (1 M $LiPF_6$ in 1:1 v/v ethylene carbonate:dimethyl carbonate), and the electrolyte was allowed to wick into the film, similar to a technique reported by Berg.[21] Chemicals used for the electrolyte mixture were purchased from Sigma Aldrich. The conductivity of the liquid electrolyte mixture was 8.2 mS cm^{-1}, as measured by a liquid conductivity meter calibrated using potassium chloride. An argon-filled glovebox with ∼2 ppm water was used for impedance measurements in the dry state, and samples were allowed to equilibrate until a stable impedance response was observed (∼1 week). These samples are referred to as "dry" samples. The ac amplitude was 100 mV to improve the signal-to-noise ratio at high impedance. A linear sweep of the LbL assembly from −100 to 100 mV gave a linear current response, confirming that impedance measurements at this amplitude are appropriate. Equivalent circuits used in data analysis are described in the Supporting Information.

Results and Discussion

To explore conditions under which the porous morphology is formed from multilayers of LPEI and PAA, two parameters

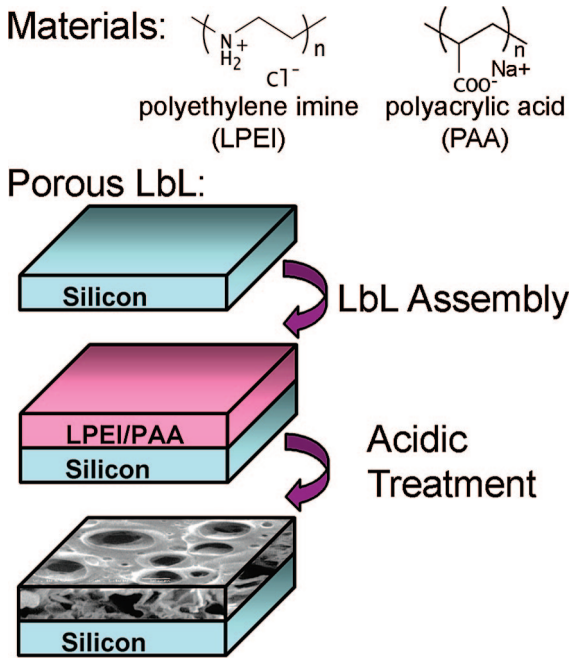

Figure 1. Porous LbL assemblies are created in a two-step procedure. First, LbL assembly is performed on a silicon (or ITO-coated glass) substrate to generate a 30-bilayer thin film, and then the LbL thin film is immersed in acidic solution. Polyelectrolytes used in this study, LPEI and PAA, are partially or fully charged depending on assembly or postassembly treatment pH.

are investigated: assembly pH (3−6) and postassembly treatment pH (1.75−3). Following assembly, LbL films of LPEI/PAA were immersed in acidic solution for 20 min; as a control, a separate set of untreated films were reserved. This immersion in acidic solution will be referred to as the "postassembly treatment" step. Samples were thermally cross-linked following the postassembly treatment step, where partial amidation of LPEI and PAA occurs above 115 °C.[47] This amidation step does not appear to modify the morphology. Figure 1 describes the materials used and the pore-formation procedure; all films addressed here consist of 30 bilayers ($(LPEI/PAA)_{30}$).

Microscopy. Tapping mode AFM was performed upon LPEI/PAA films to characterize the surface structure before and after postassembly treatment (Figure 2). Height images of untreated pH 4 and 5 LPEI/PAA LbL films appeared smooth (4 ± 2 nm), while treatment in acidic solution changed the surface of the film dramatically. Observed features include isolated pores less than 100 nm in diameter (postassembly treatment pH 2), rough and mottled bumps (pH 2.5 and 2.75), and isolated craterlike micron-scale pores (pH 3). Images obtained for treatment pH 1.75 were difficult to analyze for pore size owing to the radius of curvature of the probe tip (∼10 nm). In general, feature size increases with increasing postassembly treatment pH. Of note, roughness measurements of films treated postassembly at pH 2.5 and 2.75 were the largest (presented in the following section) among the sample set; the observed surface morphology and roughness at these conditions suggests possible competition or transition between nano- and microscale features. Also, in two cases (assembly pH 3 and 6, not shown), no evidence of pore formation was observed upon acidic treatment: the surface remained smooth and featureless, identical to control samples.

To complement findings from AFM, optical microscopy was used to observe the surface features of LPEI/PAA multilayers (Figure 1 of Supporting Information). Only microscale features are visible using this technique, but features for pH 4 and 5 LPEI/PAA films are visible when treatment pH is greater than 2.5. Also, no features were observed for systems assembled at pH 3 or 6.

The structure of the porous LbL films was further investigated using top-down and cross-section SEM of pH 5 LPEI/PAA multilayers postassembly treated at various pH (Figure 3). As before, a significant range of architectures is observed. Films treated at pH 1.75 yield nanoporous morphology, though images gathered here are not sufficient to determine pore size, and surface images suggest stress-related wrinkling: at this postassembly treatment condition, the film tends to delaminate from its substrate. Films treated at pH 2 give an interesting heterogeneous structure, comprised of two distinct regions with different pore length scales. Treatment pH 2.25 also gives a highly porous, heterogeneous structure (77% pore volume, calculated in the following section), treatment pH 2.50 and 2.75 appear to possess a collapsed structure, and those treated at pH 3 have isolated, craterlike pores about 5 μm in diameter.

The structure created and observed from postassembly treatment at pH 2 and 2.25 is of particular interest and appears similar to a phase inversion or asymmetric membrane, a structure that is useful for filtration and drug delivery applications.[48,49] To the best of the authors' knowledge, this structure has yet to be reported for LbL films. At pH 2 the dense, nanoporous region (top layer) appears to have a relatively smooth skin (120 nm rms roughness) with pores ∼100 nm in size (from AFM, Figure 2); the bottom region, at the substrate−LbL interface, is microporous. Also, at this combination of treatment and assembly conditions, a high pore volume was observed (72%, calculated in the following section). This asymmetric morphology has not been observed in PAH/PAA or other multilayer systems.

The reason for the formation of this asymmetric structure is not yet understood, but the two regions of porosity suggest that two different time scales, possibly related to the diffusion of protons (localized pH) or the interdiffusion of polyelectrolyte during either the assembly or postassembly process, may contribute. When the LbL film is first exposed to acidic solution, nanopores may quickly form, thus creating a "skin", because the outer LbL surface is in primary contact with the acidic solution. The rapid formation of this skin could be enabled by the high mobility of the LPEI polycation; alternatively, the exponential growth of the LPEI/PAA film may lead to a thicker layer of PAA on the outer surface, which neutralizes immediately upon exposure to low pH water. With further exposure, the acidic solution is able to penetrate the newly formed "skin" and may cause further rearrangement on a much slower time scale, generating microscale pores, possibly via the dissolution or loss of polyelectrolyte constituents.[29] Similar phenomena are observed in phase inversion processes for membrane formation, in which water acts as a precipitant in the exposure of a film of polymer and polar solvent, generating an outer skin layer, followed by diffusion of water into the film and diffusion of water and polar solvent out of the film, thus enabling the generation of large micropores.[50]

Porosity and Surface Roughness. Given previous reports of LbL films of PAH and PAA,[28] film thickness is expected to increase when transitioning from a continuous to a porous LbL film. The thickness, t, of each system was measured before (t_{before}) and after (t_{after}) the postassembly treatment step and amidation. Following the acidic treatment step, an increase in t was often observed; this increase was used to calculate the pore (or void) volume as $100(t_{after} - t_{before})/t_{after}$, assuming no change in mass.[28] A detailed derivation of this expression is provided in Supporting Information. Figure 4a describes the pH dependency of pore volume within various LPEI/PAA LbL systems. Films assembled at pH 3 exhibit a calculated pore volume near or below 0%, suggesting that the film is either

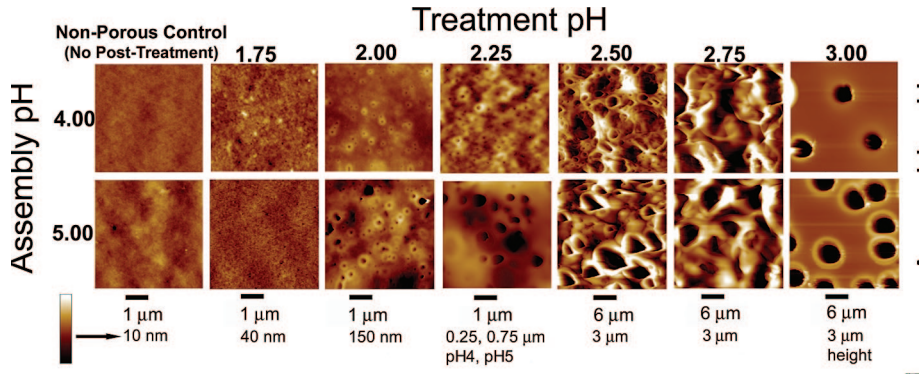

Figure 2. Tapping mode atomic force microscopy height images of pH 4 and 5 LPEI/PAA multilayers treated at varying pH. Nonporous control samples were left untreated. Pore sizes range from tens of nanometers to ~5 μm.

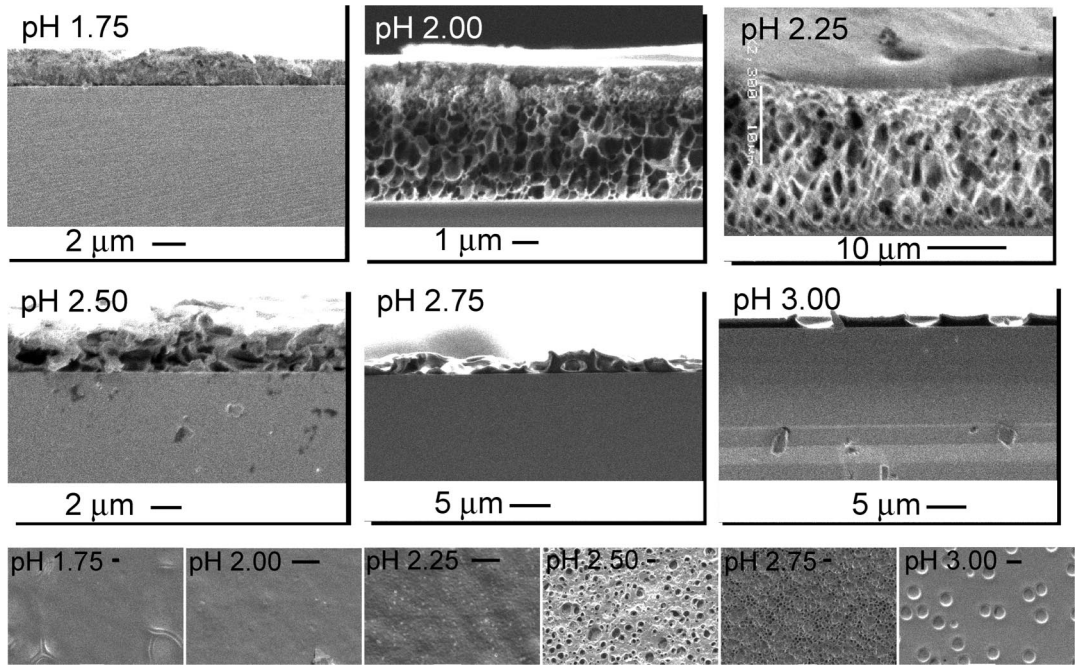

Figure 3. SEM cross-section (upper two rows) and top-down images (bottom row) of pH 5 LPEI/PAA multilayers treated at varying pH. Conditions are 2−5 keV. Top-down image scale bars are 5 μm. Samples were coated with 100 Å of Au−Pd.

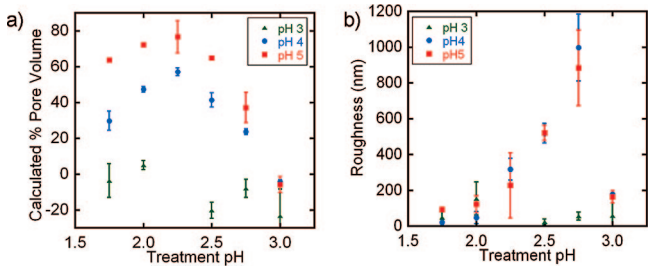

Figure 4. Pore volume (a) and surface roughness (b) of LPEI/PAA multilayers assembled at pH 3−5 and postassembly treated at pH 1.75−3.00. Thickness and roughness were measured using profilometry of dried LbL films. Pore volume was calculated using $100(t_{after} - t_{before})/t_{after}$,[28] described within the text and Supporting Information.

nonporous or losing mass. For those assembled at pH 4 or 5, film thickness doubled or tripled for postassembly treatments of pH 2 and pH 2.25. Maximum calculated pore volumes of 57% and 77% occurred when $(LPEI/PAA)_{30}$ was assembled at pH 4 and 5, respectively, and was treated at pH 2.25. Calculated pore volume decreases below treatment pH 2, and below pH 1.75, the film delaminates from its silicon substrate. Above treatment pH 3, the pore volume is negligible (~0%). Visually, films treated at pH 2.5 and below were opaque while those above 2.75 were optically clear; opacity development was visually observed during the postassembly pH treatment immersion step. Films assembled at pH 6 were so thin (<10 nm) that profilometry could not be used; additionally, ellipsometry yielded thicknesses with large sample-to-sample deviation, indicating nonuniformity of the film samples. For this reason, only films assembled between pH 3 and 5 are considered.

In a similar study,[28] multilayers of PAH and PAA were immersed in acidic solution, and an increase in thickness or porosity was also observed. The maximum reported pore volume for PAH/PAA systems was 66%,[28] when PAA and PAH assembly pH were 3.5 and 7.5, respectively, and postassembly treatment pH was 2.4. Of note, at these assembly conditions, both PAA and PAH are partially ionized and the assembled PAH/PAA multilayers produced the thickest layer pairs.[28] Similarly here, the most porous LPEI/PAA multilayer systems were produced from conditions (assembly pH = 4 or 5) in which LPEI ($pK_a \sim 6$) and PAA ($pK_a \sim 5.5-6.5$) are partially ionized, yielding the thickest layers (30 nm per layer pair).[39] Also at these conditions, LPEI is known to be particularly mobile within the layer-by-layer film during the assembly process and is capable of exchange and internal diffusion;[44,45] LPEI/PAA LbL

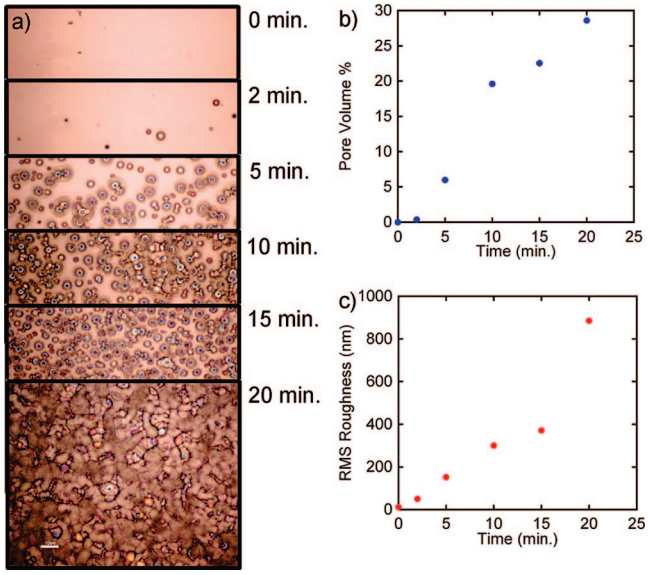

Figure 5. Optical microscopy (a) of dried pH 5 LPEI/PAA multilayers that had been treated in pH 2.75 water for various exposure times. The porosity (b) and surface roughness (c) also change with time, as measured using profilometry.

films exhibit exponential growth profiles, a common indicator of this phenomena.

The root-mean square (rms) surface roughness of each LPEI/PAA film was measured using profilometry after the postassembly treatment step (see Materials and Methods) to give an idea of the effect of varying assembly and postassembly treatment pH (Figure 4b). Though untreated control samples were uniformly smooth (4 ± 2 nm), the surface roughness of films treated with acidic solution was 5−250 times higher. Films assembled at pH 3 were 50−150 nm rough, though response appeared independent of treatment pH; in contrast, the roughness of films assembled at pH 4 and 5 increased with increasing treatment pH, reaching nearly 1 μm rms roughness at treatment pH 2.75. All films postassembly treated at pH 3 exhibited roughnesses less than 200 nm. Overall, film thickness ranged from 1 to 7 μm depending on assembly and treatment pH conditions, and in some cases, (e.g., postassembly treatment pH 2.75) rms roughness was on the order of film thickness.

Given the porosity and roughness responses observed after 20 min of acidic treatment (Figure 4), the effect of immersion time is considered an important parameter. Using optical microscopy and profilometry, surface morphology, porosity and roughness were monitored as a function of treatment time (Figure 5). Optical microscopy is a useful tool for monitoring the development of micron-scale surface features. Untreated pH 5 $(LPEI/PAA)_{30}$ films appear smooth and featureless (0 min), whereas after 5 min of exposure to pH 2.75 water, isolated micron-scale pores appear and surface roughness and pore volume increase. As exposure time further increases, the number of pores increases until they merge together after 20 min. Pore volume and roughness climbs to 29% and 900 nm, respectively. In this particular system (treatment pH 2.75), the effect of longer exposure times is unexplored, though volume and roughness data indicates that further structural change is possible. The kinetics of the porous transition in LPEI/PAA films has also been studied via FTIR spectroscopy[37,38] (Supporting Information).

A similar experiment was performed for pH 5 $(LPEI/PAA)_{30}$ LbL films treated at pH 2, where the pore volume was tracked for 6 h of exposure (Figure 2 of Supporting Information). At this post-treatment pH, the bulk of the porous transition occurs much more rapidly than the pH 2.75 study. Once immersed in pH 2 solution, pore volume jumps to ~72% after 2 min and remains constant even after 6 h. From optical microscopy and AFM (not shown) the surface remains smooth for all exposure times. The order magnitude difference in time response between pH 2 and pH 2.75 treatments suggests that the formation of porous structure may follow different kinetics with respect to treatment pH, implying differences in either driving force for rearrangement or chain mobility, and is a subject of further study.

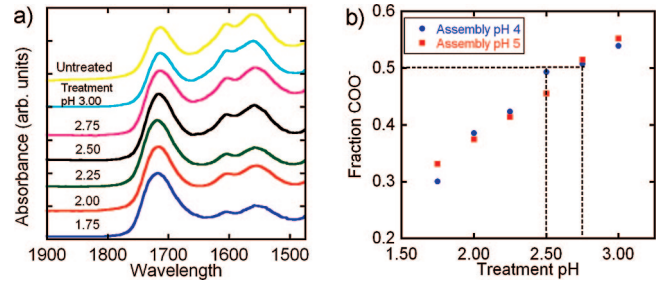

Figure 6. FTIR spectra (a) of pH 5 LPEI/PAA multilayers treated at varying postassembly pH. The fraction of COO^- (b), or fraction of AA units that are ionized, was calculated from the absorbance bands at 1560 and 1715 cm^{-1} of pH 4 or 5 LbL films treated at varying pH. The lines indicate the $pK_{1/2}$ of PAA, where 50% of PAA monomer units are ionized near postassembly treatment pH 2.5 or 2.75.

FTIR Spectroscopy. To further understand the role of electrostatic interactions and the ionization of polyelectrolytes within the LbL film, FTIR spectroscopy of LPEI/PAA LbL films atop an IR-transparent silicon substrate in a nitrogen-purged environment was performed. LbL multilayers assembled at pH 4 and 5 were both investigated, but for brevity, only assembly pH 5 is shown (Figure 6a). For all systems, three peaks (1715, 1603, and 1560 cm^{-1}) were observed in the region investigated (1500−1900 cm^{-1}). The peak at 1603 cm^{-1} corresponds to a secondary amine,[45,51] the broad peak at 1715 cm^{-1} is attributed to neutral PAA (COOH) which may be present in its "dimerized" or "free" state, (1710 or 1740 cm^{-1}, respectively),[51,52] and the peak observed at 1560 cm^{-1} suggests that some amount of PAA is ionized (COO^-).[51,53] Qualitatively, the COO^- peak absorbance at 1560 cm^{-1} increases as postassembly treatment pH increases from 1.75 to 3.00. Also, the FTIR spectra of an untreated pH5 LPEI/PAA film appeared similar to that of a pH 5 film treated at pH 3.00. Assuming that COO^- and COOH peaks have similar extinction coefficients,[54] the fraction of ionized PAA monomer units was calculated using $Abs_{1560}/(Abs_{1715} + Abs_{1560})$.[55] Performing the calculation for systems assembled at pH 4 or 5 (Figure 6b), PAA ionization within LbL films ranges from 30 to 54% or 33 to 55%, respectively. For comparison, PAA within an untreated pH 4 or 5 LPEI/PAA film was 54 or 55% ionized, respectively. Amide peaks (~1670 cm^{-1}) associated with heat treatment[47] were not observed, suggesting that the PAA absorbance may overshadow the amide response owing to a small degree of amide cross-linking.

Of note, as determined by Choi and co-workers,[55] the $pK_{1/2}$ of PAA in solution (pH = 5.5−6.5) and in an LbL film (pH = 2.2−3.0) are known to differ depending on the choice of complementary polycation, where $pK_{1/2}$ is the point at which 50% of the polymer is ionized. The depression of the pK_a or $pK_{1/2}$ of PAA within multilayer films has also been reported elsewhere.[56−58] This behavior is attributed to favorable electrostatic interactions, where PAA further ionizes in the presence of basic polycations, depressing the $pK_{1/2}$. In this work, the estimated $pK_{1/2}$ of PAA within pH 4 and 5 LPEI/PAA multilayers is 2.5−2.75, as emphasized by the tie lines in Figure 6b.

Seeking to implement a similar analysis to that of PAA, the ionization and neutralization of neat solution-cast LPEI from

pH 2 to 6 was investigated (Figure 3 of the Supporting Information). With increasing pH, two peaks emerge (1605 and 1450 cm^{-1}), which may be attributed to NH deformation.[51] Unfortunately within the LPEI/PAA multilayer film, quantifying the role of LPEI proved difficult because the peaks of interest overlap with that of PAA. However, the second peak observed in Figure 6a (1603 cm^{-1}) coincides with that of LPEI alone, confirming its presence within the multilayer film.

Given the pH-stimulated response of LPEI/PAA LbL multilayers, we hypothesize that the change in thickness, or the degree of pore formation, is linked to changes in charge density of LPEI and PAA: both being weak polyelectrolytes, LPEI and PAA will ionize and deionize, respectively, in response to localized acidic pH. At pH 4 and 5, pure-component solutions of LPEI or PAA are known to be partially charged (solution $pK_{1/2} = 6$ and 5.5−6.5, respectively),[55,59,60] and LbL assemblies of LPEI and PAA constructed under these conditions yield lightly electrostatically cross-linked films containing many loops and tails.[39] When the LbL film is immersed in acidic solution (i.e., treated at pH < 3), the protonic environment neutralizes PAA and ionizes LPEI. The stability of this electrostatically cross-linked film becomes compromised, as cross-links are disrupted (via the neutralization of PAA) and excess positive charge accumulates (via the ionization of LPEI); to some extent, loss of constituent polyelectrolytes is also possible.[29] Electroosmotic forces may also play a significant role in the development of the observed porous structures, where the ionization of polyelectrolytes (i.e., LPEI) requires the incorporation of counterions for electroneutrality. Such intake of counterions could cause significant swelling and morphological rearrangement.

In more extreme cases, when postassembly treatment pH is less than 2.0, excess rearrangement leads to the deconstruction or delamination of the LbL film. A similar mechanism is proposed for microporous PAH/PAA systems.[28] Of note, the deconstruction of films at pH < 2 conflicts with the assumption of constant mass in calculating pore volume. Under these conditions, the real pore volume is expected to be greater than values estimated from the equation described in the previous section, % pore volume $= 100(t_{after} - t_{before})/t_{after}$.

We also investigated whether the porous transition in LPEI/PAA films was reversible, as had been reported for PAH/PAA LbL systems.[24] LPEI/PAA multilayers, assembled at pH 4, were immersed in water of pH 2 and dried with high-velocity air; then, the porous film was immersed in Milli-Q water (pH ∼ 5.5) for varying amounts of time (2 min to 1 h). These alternating immersion steps were repeated three times, and the thickness and surface morphology of the film following each step was studied using profilometry and AFM (not shown). We would expect the thickness to increase or decrease with the creation or deconstruction, respectively, of the porous architecture; however, results indicate that the transition is not reversible, with no significant change in film thickness (±5%) or observed surface morphology. Of note, the thermal cross-linking step was omitted in the reversibility study. Indeed, the lack of reversibility indicates that the cross-linking heat treatment step may be un-needed.

Ionic Conductivity and Impedance Spectroscopy. It was desired to evaluate the potential of the observed structures as a porous support for nonaqueous liquid electrolyte; furthermore, impedance studies can yield important information about pore continuity and connectivity within the generated porous films. Using impedance spectroscopy, we expect to observe different modes of ion transport and to determine the conductivity of the porous, liquid-filled LbL structure. The pH 5 LPEI/PAA LbL films were assembled atop glass substrates patterned with parallel stripes of ITO 3 mm wide and treated at varying

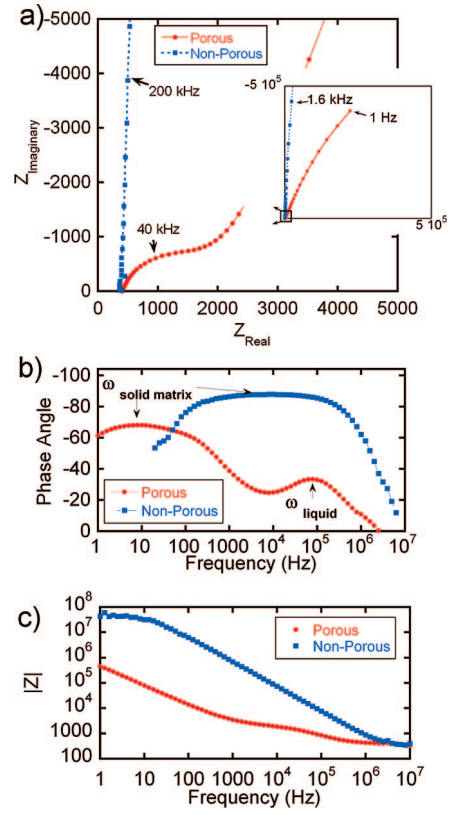

Figure 7. Nyquist (a) phase angle vs frequency (b) and |Z| vs frequency (c) plots of porous and nonporous pH 5 LPEI/PAA multilayers, both exposed to electrolyte mixture. Porous films yielded two semicircles in the Nyquist plot, where the high-frequency semicircle is presented in (a) and the low-frequency semicircle is presented in the inset. Porous films exhibit two time constants, shown in the phase angle vs frequency plot (b), whereas nonporous films yield one. Additional views of the Nyquist plot (a) are given in the Supporting Information.

assembly pH as described before. Following LbL assembly and thermal cross-linking, gold electrodes were evaporated atop the LbL film to yield an ITO|LbL|Au cell. The edge of the cell was placed in a shallow dish of electrolyte comprised of 1:1 v/v ethylene carbonate:dimethyl carbonate and 0.3 M lithium hexafluorophosphate ($LiPF_6$), where the measured electrolyte mixture conductivity was 8.2 mS cm^{-1}. Nano- and microporous LbL films readily uptake the solution, and progress may be monitored visually due to the corresponding change in the film's refractive index.[21] The electrolyte was able to wick up to 1 cm in height into the film, and the film changed in optical clarity (from opaque to nearly clear).

Impedance spectroscopy in a dry, argon-filled glovebox was performed on each system as well as a nonporous control. Typical responses for both electrolyte-treated systems are described in Figure 7. In the Nyquist and phase angle vs frequency plots, the nonporous LbL film yields a single semicircle and time constant, respectively, whereas the porous film gives two. These impedance responses may be modeled by two different equivalent circuits (Figure 5 of Supporting Information) further described within the Supporting Information.

For each semicircle or time constant, a conductivity was calculated (Figure 8). The nonporous LbL system soaked in electrolyte as a control yielded a single conductivity of $(2.3 \pm 0.2) \times 10^{-9}$ S cm^{-1}; in contrast, porous electrolyte-filled systems demonstrated two conductivities, $\sim 10^{-6}$ and 10^{-9}−10^{-10} S cm^{-1}. The highest observed conductivity, $(1.5 \pm 0.8) \times 10^{-6}$ S cm^{-1}, occurred at postassembly treatment pH 2, which was 72% porous.

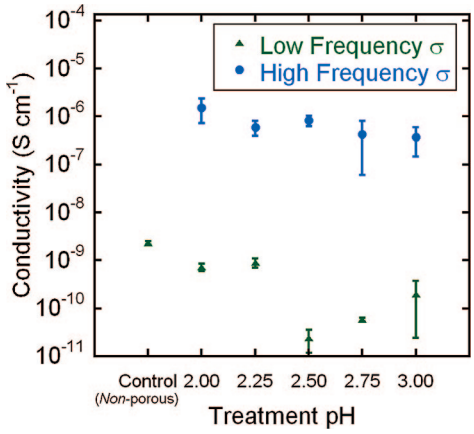

Figure 8. Conductivity of electrolyte-filled porous pH 5 LPEI/PAA multilayers postassembly treated at varying pH. The control is a nonporous pH 5 film exposed to electrolyte. Here, conductivity was calculated from R_2 and R_3, which were estimated using the equivalent circuits described in the Supporting Information.

We hypothesize that the two conductivities observed in porous, liquid-filled multilayers are each attributed to transport in separate phases: the higher conductivity (10^{-6} S cm^{-1}) is linked to ion transport within the liquid-filled pores (i.e., "liquidlike"), and the lower conductivity ($\sim 10^{-9}$ S cm^{-1}) is attributed to transport through the solid matrix (i.e., "solidlike"). The latter hypothesis is further supported by the fact that the lower conductivity in porous multilayers (10^{-9}–10^{-10} S cm^{-1}) is comparable to that observed in the nonporous electrolyte-soaked control (10^{-9} cm^{-1}). Similar impedance spectra and equivalent circuits have been reported elsewhere for analogous systems.[61–63] For porous sulfonated polysulfone membranes, the two reported semicircles in the Nyquist response were separately attributed to the conductivity of the electrolyte and the membrane.[61] Also, in membranes with a skin layer, others have attributed the two relaxations to ion transport in the skin layer and the microporous sublayer.[62] And finally, in the case of poor wetting, electrolyte-filled conventional porous separators such as Celgard sometimes exhibit two semicircles, corresponding to bulk electrolyte and interfacial impedance.[63]

As might be expected, the conductivity of LPEI/PAA multilayers increases when the LbL film is soaked in electrolyte. In this work, a dry (0% RH) conductivity of $(2.3 \pm 0.2) \times 10^{-9}$ S cm^{-1} was observed for untreated pH 5 LPEI/PAA multilayers soaked in electrolyte, which is an 80-fold improvement over previously reported[39] untreated pH 5 LPEI/PAA multilayers without electrolyte ($\sigma = (2.8 \pm 0.2) \times 10^{-11}$ S cm^{-1} (17% RH)). We attribute this increase to the addition of liquid electrolyte which is thought to plasticize the nonporous LbL film (improving the mobility of the charge carrier) and to dope the matrix with lithium cations (increasing the number of charge carriers).

As for the porous, liquid-filled multilayers, the value of the high-frequency conductivity presents an interesting paradox; the conductivity of the liquid electrolyte alone is 8.2 mS/cm, but the high-frequency conductivity observed in porous multilayers is 1000 times lower. A few possible explanations may address this discrepancy. One cause for the low ionic conductivity in such highly porous films could be the formation of pores that are not well interconnected. The isolated pockets of electrolyte-filled pores may still conduct ions but are hindered by a lack of interconnectivity (i.e., not percolating). Given the large magnitude of discrepancy, this explanation seems most plausible. Initial calculations of toruosity based upon an analysis presented by Song et al.[63] give tortuosity values greater that 600, which appears to be unusually large and supports the possibility of isolated, nonpercolative pores. Another means of error is that conductivity was calculated using a cell constant (L/A) derived from the distance between the electrodes, L, and the area of the electrodes, A. However, this assumption may fail if the real path length, L_{real}, is tortuous[64] or if the effective area, A_{real}, is limited by the presence of a nanoporous "skin". Another explanation for this discrepancy is that the nonaqueous liquid electrolyte may not fully wet the LbL matrix, which may prevent the porous support from being fully filled. However, preliminary results suggest that some degree of wetting is possible: the advancing contact angle of the electrolyte mixture on a nonporous pH 5 LPEI/PAA surface was 43°, which decreased to 30° 1 min later. On a porous pH5 LPEI/PAA surface (postassembly treatment pH 2), the advancing contact angle was 56°, decreasing to 40° after 1 min. Here the relative increase in contact angle (porous vs nonporous) may be attributed to increasing surface roughness.

Conclusion

The origin and modulation of the porous transition of linear poly(ethylenimine)/poly(acrylic acid) multilayers was investigated with regard to assembly pH and postassembly treatment using profilometry, FTIR spectroscopy, and various forms of microscopy. Results suggest that the charge density and electrostatic cross-link density of the multilayer play key roles in the porous transition. The maximum observed pore volume was 77%, which occurred at assembly pH 5 and postassembly pH 2.25. An optimum "window" for creating porous structure in LPEI/PAA multilayers was identified. The porous transition was linked to neutralization of PAA and ionization of LPEI, which disrupts electrostatic cross-links and causes electrostatic repulsion and may also contribute to electro-osmotic swelling. Pore size increased from tens of nanometers to microns as postassembly treatment pH increased from 1.75 to 3.00.

For the first time, an asymmetric membrane LbL structure was reproducibly observed with postassembly treatment pH 2.00 and 2.25. It is hypothesized that the formation of a thin upper skin layer with fine pores followed by a thick, microporous layer is in some way enabled by the high degree of mobility of LPEI or the interdiffusing nature of the LPEI/PAA assembly pair. The origin or formation mechanism for this particular membrane is not well understood and is a subject of future research. The observed asymmetry may be of use in filtration, drug delivery, or catalysis applications.

To evaluate its potential use as an ultra thin separator or electrolyte support, porous pH 5 LPEI/PAA multilayers were immersed in a nonaqueous electrolyte cocktail to yield a liquid-filled porous matrix. Preliminary results indicate that porous LPEI/PAA LbL films may be produced as thin as 1 μm, which is much thinner than conventional separators.[40] Impedance spectroscopy revealed two time constants, indicative of two modes of ion transport. The high-frequency conductivity, 10^{-6} S cm^{-1}, was attributed to ion transport in the liquid-filled pores, and the low-frequency conductivity, 10^{-9} S cm^{-1}, was linked to the LbL matrix. Potential means of improving conductance include improving pore connectivity beyond a percolation threshold, using different electrolytes, or creating thinner LbL films. Structures described in this work provide a guide to modulating and controlling pore size, surface area, roughness, and transport in porous LbL thin films from weak polyelectrolytes. The ability to tune the porous film structures is promising for applications in separations membranes, reactive membranes, and electrodes.

Acknowledgment. We thank the Dupont-MIT Alliance and the Institute of Soldier Nanotechnology for funding as well as the Center for Materials Science and Engineering for facilities. J.L.

thanks the National Science Foundation Graduate Fellowship. We thank Professors M. Rubner and R. Cohen for their helpful discussions.

Supporting Information Available: Derivation of pore volume equation, monitoring of porous transition using FTIR spectroscopy discussion, impedance spectroscopy, and FTIR spectra of solution-cast LPEI at varying pH; optical microscopy of LPEI/PAA multilayers assembled at pH 3−6, treated at pH 1.75−3, and a control. This material is available free of charge via the Internet at http://pubs.acs.org.

References and Notes

(1) Stein, A.; Melde, B. J.; Schroden, R. C. *Adv. Mater.* **2000**, *12* (19), 1403–1419.
(2) Gelb, L. D.; Gubbins, K. E.; Radhakrishnan, R.; Sliwinska-Bartkowiak, M. *Rep. Prog. Phys.* **1999**, *62* (12), 15731659..
(3) Barton, T. J.; Bull, L. M.; Klemperer, W. G.; Loy, D. A.; McEnany, B.; Misono, M.; Monson, P. A.; Pez, G.; Scherer, G. W.; Vartuli, J. C.; Yaghi, O. M. *Chem. Mater.* **1999**, *11* (10), 2633–2656.
(4) Freyman, T. M.; Yannas, I. V.; Gibson, L. J. *Prog. Mater. Sci.* **2001**, *46* (3−4), 273–282.
(5) Cohen, R. E. *Curr. Opin. Solid State Mater. Sci.* **2000**, *4* (6), 587590..
(6) Peinemann, K.-V.; Nunes, S. P. Membrane Application. In *Handbook of Porous Solids*; Wiley VCH: Weinheim, Germany, 2002; Vol. 4, pp 2507−2532.
(7) Guliants, V. V.; Carreon, M. A.; Lin, Y. S. *J. Membr. Sci.* **2004**, *235* (1−2), 53–72.
(8) Svec, F. *J. Sep. Sci.* **2004**, *27* (17−18), 1419–1430.
(9) McKeown, N. B.; Budd, P. M. *Chem. Soc. Rev.* **2006**, *35* (8), 675–683.
(10) Lee, J.; Kim, J.; Hyeon, T. *Adv. Mater.* **2006**, *18* (16), 2073–3094.
(11) Szumski, M.; Buszewski, B. *J. Sep. Sci.* **2007**, *30* (1), 55–66.
(12) Decher, G.; Hong, J. D.; Schmitt, J. *Thin Solid Films* **1992**, *210−211* (2), 831–835.
(13) Decher, G. *Science* **1997**, *277* (5330), 1232–1237.
(14) Lefaux, C. J.; Mather, P. T. In *Build-up of Multilayered Thin Lines Using Sequential Adsorption of Polymers in Microfluidic Channels*; Materials Research Society Symposium Proceedings, 2004; Materials Research Society: Warrendale, PA, 2004; pp 47−49.
(15) Ding, B.; Fujimoto, K.; Shiratori, S. *Thin Solid Films* **2005**, *491* (1−2), 23–28.
(16) Mueller, K.; Quinn, J. F.; Johnston, A. P.; Becker, M.; Greiner, A.; Caruso, F. *Chem. Mater.* **2006**, *18* (9), 2397–2403.
(17) Shiratori, S.; Rubner, M. F. *Macromolecules* **2000**, *33* (11), 4213.
(18) Dubas, S. T.; Schlenoff, J. B. *Macromolecules* **1999**, *32* (24), 8153–8160.
(19) Lutkenhaus, J. L.; McEnnis, K.; Hammond, P. T. *Macromolecules*. **2007**, ASAP.
(20) Zhai, L.; Nolte, A. J.; Cohen, R. E.; Rubner, M. F. *Macromolecules* **2004**, *37* (16), 6113–6123.
(21) Berg, M. C.; Zhai, L.; Cohen, R. E.; Rubner, M. F. *Biomacromolecules* **2006**, *7* (1), 357–364.
(22) Zhai, L.; Cebeci, F. C.; Cohen, R. E.; Rubner, M. F. *Nano Lett.* **2004**, *4* (7), 1349–1353.
(23) Zhai, L.; Berg, M. C.; Cebeci, F. C.; Kim, Y.; Milwid, J. M.; Rubner, M. F.; Cohen, R. E. *Nano Lett.* **2006**, *6* (6), 1213–1217.
(24) Hiller, J. A.; Mendelsohn, J. D.; Rubner, M. F. *Nat. Mater.* **2002**, *1*, 59–63.
(25) Hiller, J.; Rubner, M. F. *Macromolecules* **2003**, *36* (11), 4078–4083.
(26) Lowman, G. M.; Hammond, P. T. *Small* **2005**, *1* (11), 1070–1073.
(27) Takenaka, S.; Maehara, Y.; Imai, H.; Yoshikawa, M.; Shiratori, S. *Thin Solid Films* **2003**, *438−439*, 346–351.
(28) Mendelsohn, J. D.; Barret, C. J.; Chan, A. J. P.; Mayes, A. M.; Rubner, M. F. *Langmuir* **2000**, *16* (11), 5017–5023.
(29) Wang, B.; Liu, L.; Chen, L.; Feng, J.; Changyou, G. *ChemPhysChem* **2006**, *7*, 590–596.
(30) Fery, A.; Scholer, B.; Cassagnearu, T.; Caruso, F. *Langmuir* **2001**, *17*, 3779–3783.
(31) Li, Q.; Quinn, J. F.; Caruso, F. *Adv. Mater.* **2005**, *17* (17), 2058–2062.
(32) Wang, Y.; Caruso, F. *Chem. Commun.* **2004**, 1528–1529.
(33) Wang, Y. F. C. *Adv. Funct. Mater.* **2004**, *14* (10), 1012–1018.
(34) Li, Q.; Quinn, J. F.; Wang, Y.; Caruso, F. *Chem. Mater.* **2006**, *18* (23), 5480–5485.
(35) Wang, Y.; Caruso, F. *Chem. Mater.* **2006**, *18* (17), 4089–4100.
(36) Wang, Y. F. C. *Adv. Mater.* **2006**, *18* (6), 795–800.
(37) Tokuhisa, H.; Hammond, P. T. *Adv. Funct. Mater.* **2003**, *13* (11), 831–839.
(38) Lowman, G. M.; Tokuhisa, H.; Lutkenhaus, J. L.; Hammond, P. T. *Langmuir* **2004**, *20* (22), 9791–9795.
(39) DeLongchamp, D. M.; Hammond, P. T. *Chem. Mater.* **2003**, *15* (5), 1165–1173.
(40) Zhang, S. S. *J. Power Sources* **2007**, *164* (1), 351–364.
(41) Yoo, P. J.; Zacharia, N. S.; Doh, J.; Hammond, P. T. *ACS Nano* **2008**, *2*, 561–571.
(42) Picart, C.; Mutterer, J.; Richert, L.; Luo, Y.; Prestwich, G. D.; Schaaf, P.; Voegel, J. C.; Lavalle, P. *Proc. Natl. Acad. Sci. U.S.A.* **2002**, *99* (20), 12531–12535.
(43) Porcel, C.; Lavalle, P.; Ball, V.; Decher, G.; Senger, B.; Voegel, J. C.; Schaaf, P. *Langmuir* **2006**, *22* (9), 4376–4383.
(44) Yoo, P. J.; Nam, K. T.; Qi, J.; Lee, S.-K.; Park, J.; Belcher, A. M.; Hammond, P. T. *Nat. Mater.* **2006**, *5*, 234–240.
(45) Zacharia, N. S.; DeLongchamp, D. M.; Modestino, M.; Hammond, P. T. *Macromolecules* **2007**, *40* (5), 1598–1603.
(46) Zacharia, N. S.; Modestino, M.; Hammond, P. T. *Macromolecules* **2007**, *40* (26), 9523–9528.
(47) Stair, J. L.; Harris, J. J.; Bruening, M. L. *Chem. Mater.* **2001**, *13* (8), 2641–2648.
(48) Feng, X.; Huang, R. Y. M. *Ind. Eng. Chem. Res.* **1997**, *36* (4), 1048–1066.
(49) Herbig, S. M.; Cardinal, J. R.; Korsmeyer, R. W.; Smith, K. L. *J. Controlled Release* **1995**, *35* (2−3), 127–136.
(50) Ahmad Fauzi Ismail, L. P. Y. *J. Appl. Polym. Sci.* **2003**, *88* (2), 442–451.
(51) Bellamy, L. J. *The Infra-red Spectra of Complex Molecules*; Chapman and Hall: London, 1975; pp 183−200.
(52) Lee, J. Y.; Painter, P. C.; Coleman, M. M. *Macromolecules* **1988**, *21* (2), 346–364.
(53) Lu, X.; Weiss, R. A. *Macromolecules* **1995**, *28* (9), 3022–3029.
(54) Xie, A. F.; Granick, S. *Macromolecules* **2002**, *35* (5), 1805–1813.
(55) Choi, J.; Rubner, M. F. *Macromolecules* **2005**, *38* (1), 116–124.
(56) Petrov, A. I.; Antipov, A. A.; Sukhorukov, G. B. *Macromolecules* **2003**, *36* (26), 10079–10086.
(57) Burke, S. E.; Barrett, C. J. *Langmuir* **2003**, *19* (8), 3297–3303.
(58) Rmaile, H. H.; Schlenoff, J. B. *Langmuir* **2002**, *18* (22), 8263–8265.
(59) Clark, S. L. Engineering the Microfabrication of Layer-by-Layer Polyelectrolyte Assembly. PhD, Massachusetts Institute of Technology, Cambridge, MA, 1999.
(60) Weyts, K. F.; Goethals, E. J. *Makromol. Chem., Rapid Commun.* **1989**, *10* (6), 299–302.
(61) Benavente, J.; Garcia, J. M.; Riley, R.; Lozano, A. E.; de Abajo, J. *J. Membr. Sci.* **2000**, *175*, 43–52.
(62) Coster, H. G. L. *Bioelectrochem. Bioenerg.* **1996**, *40* (2), 79–98.
(63) Song, J. Y.; Wang, Y. Y.; Wan, C. C. *J. Electrochem. Soc.* **2000**, *147* (9), 3219–3225.
(64) Abraham, K. M.; Alamgir, M. *J. Electrochem. Soc.* **1995**, *142* (3), 683–687.

MA800003X